Original Article

Mol Imaging Radionucl Ther 2024;33:156-166 *DOI:10.4274/mirt.galenos.2024.59365*

Assessment of Y-90 Radioembolization Treatment Response for Hepatocellular Carcinoma Cases Using MRI Radiomics

MRG Radiomics Kullanılarak Hepatosellüler Karsinom Olgularında Y-90 Radyoembolizasyon Tedavisine Yanıtın Değerlendirilmesi

Mennaallah Mahmoud[1], Ko-Han Lin[2], Rheun-Chuan Lee[1], Chien-an Liu[1]

[1]Taipei Veterans General Hospital, Clinic of Radiology, Taipei, Taiwan
[2]Taipei Veterans General Hospital, Clinic of Nuclear Medicine, Taipei, Taiwan

Abstract

Objectives: This study aimed to investigate the ability of radiomics features extracted from magnetic resonance imaging (MRI) images to differentiate between responders and non-responders for hepatocellular carcinoma (HCC) cases who received Y-90 transarterial radioembolization treatment.

Methods: Thirty-six cases of HCC who underwent MRI scans after Y-90 radioembolization were included in this study. Tumors were segmented from MRI T2 images, and then 87 radiomic features were extracted through the LIFEx package software. Treatment response was determined 9 months after treatment through the modified response evaluation criteria in solid tumours (mRECIST).

Results: According to mRECIST, 28 cases were responders and 8 cases were non-responders. Two radiomics features, "Grey Level Size Zone Matrix (GLSZM)-Small Zone Emphasis" and "GLSZM-Normalized Zone Size Non-Uniformity", were the radiomics features that could predict treatment response with the area under curve (AUC)= 0.71, sensitivity= 0.93, and specificity= 0.62 for both features. Whereas the other 4 features (kurtosis, intensity histogram root mean square, neighbourhood gray-tone difference matrix strength, and GLSZM normalized grey level non-uniformity) have a relatively lower but acceptable discrimination ability range from AUC= 0.6 to 0.66.

Conclusion: MRI radiomics analysis could be used to assess the treatment response for HCC cases treated with Y-90 radioembolization.

Keywords: MRI, radiomics, Y-90 radioembolization

Öz

Amaç: Bu çalışma, Y-90 transarteriyel radyoembolizasyon tedavisi gören hepatosellüler karsinomlu (HCC) olgularda manyetik rezonans görüntüleme (MRG) ile elde edilen görüntülerden çıkarılan radiomics özelliklerinin tedaviye yanıt verenler ile yanıt vermeyenler arasında ayrım yapma yeteneğini araştırmayı amaçlamaktadır.

Yöntem: Y-90 radyoembolizasyonundan sonra MRG taramaları yapılan 36 HCC olgusu bu çalışmaya dahil edildi. Tümörler MRG T2 görüntülerinden segmentlere ayrıldı ve ardından LIFEx paket yazılımı aracılığıyla 87 radiomics özelliği çıkarıldı. Tedavi yanıtı, tedaviden 9 ay sonra solid tümörlerde yanıt değerlendirme kriterleri (mRECIST) ile belirlendi.

Bulgular: mRECIST'e göre 28 olgu yanıt veren ve 8 olgu yanıt vermeyen olgulardı. İki radiomics özelliği "Gri seviye boyut bölgesi matrisi (GLSZM)-küçük bölge vurgusu" ve "GLSZM-normalize bölge boyutunun tekdüze olmaması", her iki özellik için de eğri altındaki alan (AUC)= 0,71 ve duyarlılık= 0,93 ve özgüllük= 0,62 ile tedavi yanıtını tahmin edebilen radiomics özellikleriydi. Diğer 4 özellik (kurtozis, yoğunluk histogramı ortalama karekökü, komşuluk gri ton farklılık matrisi gücü, GLSZM normalize gri seviye tekdüze olmaması) ise nispeten düşük ancak kabul edilebilir bir ayrım yeteneği aralığına sahiptir ve AUC= 0,6 ile 0,66 arasındadır.

Sonuç: MRG radiomics analizi, Y90 radyoembolizasyonu ile tedavi edilen HCC vakalarında tedavi yanıtını değerlendirmek için kullanılabilir.

Anahtar kelimeler: MRG, radiomics, Y-90 radyoembolizasyonu

Address for Correspondence: Ko-Han Lin MD, Taipei Veterans General Hospital, Clinic of Nuclear Medicine, Taipei, Taiwan
Phone: +0228712121 **E-mail:** khlin1979@gmail.com ORCID ID: orcid.org/0000-0002-1464-3483
Received: 19.10.2023 **Accepted:** 04.08.2024 **Epub:** 03.10.2024

Introduction

Hepatocellular carcinoma (HCC) stands as a significant contributor to cancer-related mortality worldwide, particularly prevalent in Asia and Africa (1). Yttrium-90 (Y-90) radioembolization emerges as a potent therapeutic modality for unresectable HCC, enabling precise delivery of high-dose of beta-radiation to the tumor while sparing adjacent healthy tissue (2). However, response to Y-90 radioembolization exhibits variability across patients, underscoring the importance of accurate response assessment in gauging treatment efficacy and guiding subsequent clinical decisions (3). Current response assessment criteria, such as modified response evaluation criteria in solid tumors (mRECIST), rely primarily on changes in tumor size, often falling short of capturing the nuanced treatment (4).

Radiomics, an advancing domain within medical imaging, presents a promising avenue for extracting quantitative features from medical images, potentially enhancing treatment response assessment. Moreover, radiomics delves into subtle nuances in image texture, shape, and intensity, imperceptible to the naked eye, yet likely correlated with tumor biology and treatment response (5). Notably, magnetic resonance imaging (MRI) radiomics has featured prominently in various studies predicting treatment responses in HCC patients. While some researchers have explored the utility of MRI-derived radiomics features in prognosticating response to transarterial chemoembolization (TACE) (6-10), few have examined their role in assessing response to transarterial radioembolization employing Y-90 in HCC patients (11,12). The aim of this current study is to investigate the efficacy of radiomic features extracted from MRI images in discriminating between responders and non-responder to Y-90 radioembolization in HCC patients.

Materials and Methods

Patients

A cohort of 36 patients with HCC (6 females and 30 males) were included in this study. Patients aged from (37 to 87) years with average age of 67.43 years. The patients' characteristics were shown in Figure 1. This study protocol was reviewed and approved by the Ethics Committee of Taipei Veterans General Hospital (IRB no: 2020-04-013BC, date: 13.04.2020). Informed consent was obtained from all subjects during inclusion in the study. Informed consent was obtained from all individual participants included in the study.

Imaging techniques

Planning Angiography and Technetium- 99m Macroaggregated Albumin (Tc-MAA) Single Photon Emission Computed Tomography (SPECT)/(CT)

All patients underwent a diagnostic angiogram and administration of 185 MBq (5 mCi) of Tc-MAA, followed by planar and SPECT/CT acquisitions on a hybrid SPECT/CT scanner (GE Discovery NM/CT670, USA) within one hour after Tc-MAA injection. Tc-MAA images were reconstructed on a GE Xeleris 3 workstation. The prescribed activity of the Y-90 microsphere was determined by medical internal radiation dosimetry (MIRD) model to reach a 120 Gy average dose in the target region for the glass microspheres and by partition model to reach tumor dose of 120 Gy.

Y-90 Radioembolization and Y-90 PET/MRI

All Y-90 treatments were done within 10 days after planning angiography using Y-90 glass microspheres (TheraSphere®; Boston Scientific Corp.) or Y-90 resin microspheres (SIR-Spheres®; Sirtex Medical Ltd.). After treatment, the post-Y90 internal pair production PET was obtained on a GE hybrid SIGNA PET/MRI with a maximum of two bed positions and 20-min acquisition per bed. MRI-T2 sequence was performed with 2D method, slice sequence= 6 mm, repetition time= 10000 msec, echo time= 106.88 msec, fat saturation= 3. All these scans and treatments occurred at our hospital between March 2018 and December 2021.

Radiomics Features

Images loaded to LIFEx Package versions 7.3.0 www.lifexsoft.org (13). Then images were segmented through three-dimensional semiautomatic tools in the package, and then 87 radiomic features were extracted, including

Characteristics of Patients	
Gender	M : F = 30 : 6
Age	37 – 87 years (mean: 67.43)
Lung shunt fraction (%)	2.4 – 20.6 (mead ± SD: 7.0 ± 4.3)
Treatment characteristics	
Glass (n=19)	1.1 – 7.3 GBq (mead ± SD: 3.1 ± 1.5)
Resin (n-17)	0.5 – 3.9 GBq (mead ± SD: 1.8 ± 1.2)
Bi-lobar treatment	28
Lobar treatment	4
Segmental treatment	4
Clinical features	
Child-Pugh score	A5 (n=30); A6 (n=6)
BCLC stage	B (n=26); C (n=10)
Alpha-fetoprotein	1.74 – 377340 ng/mL (median: 811)

Figure 1. Summary of patient characteristics that were included in this study

31 histogram features, 24 grey-level co-occurrence matrix Grey Level Cooccurrence Matrix (GLCM) features, 11 neighbourhood grey-level different matrix (GLRLM) features, 5 features grey-level run length matrix neighbourhood gray-tone difference matrix (NGTDM) features, and 16 Grey Level Size Zone Matrix (GLSZM) features. Figure 2 shows examples of HCC cases before and after segmentation.

Objective Response Rate (ORR)

The localized tumour response was defined as the response or progression within the radioembolization-treated liver. The response was evaluated using the mRECIST for HCC (14). Based on the best response of tumours observed on contrast-enhanced MRI or CT within 9 months after radioembolization. The ORR was defined as the sum of the complete response and the partial response. Eight cases were non-responders, while 28 cases were responders to treatment.

Statistical Analysis

The study used the Mann-Whitney U test to compare the responder and non-responder groups. The area under the curve from the receiver operating characteristic (ROC) was used to determine which features are sensitive to differentiating between responders and non-responders. The significance value for the tests was set at 0.05. All statistical tests were performed using Government of National Unity Public Social Private Partnership version 1.6.0.

Results

According to the Mann-Whitney U test, the only features with a significant difference between responders and non-responders had a significance value of 0.02 (Table 1), whereas most of the features had a significance value higher than 0.05, indicating that there was no significant difference between the two groups, as shown in Table 2. The area under curve (AUC) was significant for two features, "GLSZM-Small Zone Emphasis" and "GLSZM-Normalized Zone Size Non-Uniformity", with an AUC of 0.71, and sensitivity= 0.93 and specificity= 0.62 for both features, as presented in Table 3 and Figure 3. Four features, kurtosis, intensity histogram root mean square, NGTDM strength, and GLSZM normalized grey level non-uniformity, had relatively lower but acceptable discrimination ability, with AUCs of 0.64, 0.66, 0.6, and 0.61, respectively.

The optimal cut-off values for the two highest features to distinguish between responders and non-responders were obtained using the maximum Youden index (sensitivity + specificity- 1), as shown in Table 3. Figure 4 shows a boxplot of the significant values for the optimal cut-off values obtained using the maximum Youden index.

Discussion

Several studies have explored the radiomic features of HCC patients undergoing Y-90 radioembolization, akin to our investigation. A study by Aujay et al. (11) examined 22 cases of HCC post-Y-90 radioembolization, identifying 14 patients as non-responders and 8 as responders. They extracted 107 radiomic features from arterial-phase and portal-venous phase MRI images. Their ROC analysis highlighted four radiomic parameters (long run emphasis, minor axis length, surface area, and grey level non-uniformity on arterial phase images) as predictors of early response. However, none of the statistically significant

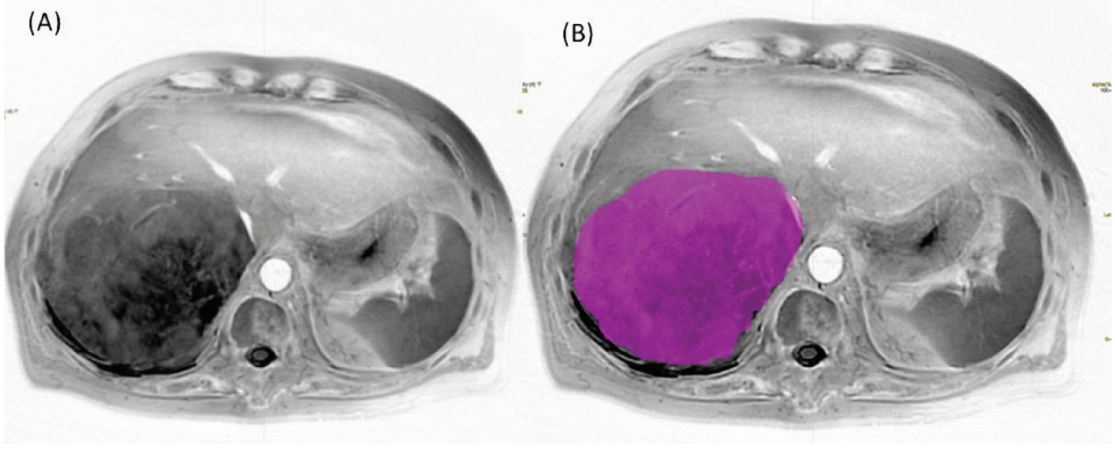

Figure 2. A case of a 58 years-old male with HCC (A) before, and (B) after segmentation in the LIFEx package
HCC: Hepatocellular carcinoma

Table 1. The results of the Mann-Whitney U test used to compare the responder and non-responder groups

Variable	Test statistics z_R	p-value
Intensity histogram mean	-0.019	0.98
Intensity histogram variance	-0.704	0.48
Intensity histogram skewness	0.209	0.83
Intensity histogram kurtosis	1.199	0.23
Intensity histogram median	0.114	0.91
Intensity histogram 10^{th} percentilei	0.514	0.61
Intensity histogram 25^{th} percentile	0.114	0.91
Intensity histogram 50^{th} percentile	-0.209	0.83
Intensity histogram75^{th} percentile	-0.45	0.65
Intensity histogram 90^{th} percentile	-0.704	0.48
Intensity histogram standard deviation	-0.305	0.76
Intensity histogram modei	-0.93	0.35
Intensity histogram mean absolute deviation	-0.704	0.48
Intensity histogram robust mean absolute deviation	-0.704	0.48
Intensity histogram median absolute deviation	-0.66	0.51
Intensity histogram coefficient of variation	-1.123	0.26
Intensity histogram quartile coefficient of dispersion	-1.16	0.24
Intensity histogram entropy $\log^{10}$	-0.74	0.46
Intensity histogram entropy $\log^{2}$	-0.74	0.46
Intensity histogram area under curve	-0.59	0.55
Intensity histogram uniformity	0.78	0.43
Intensity histogram root mean square	1.31	0.19
Intensity histogram maximum histogram gradient	-0.59	0.55
Intensity histogram maximum histogram gradient grey level	0	1
Intensity histogram minimum histogram gradient	0.59	0.55
Intensity histogram minimum histogram gradient grey level	-0.019	0.98
Histogram intensity peak discretized volume sought	0.305	0.76
HISTOGRAM global intensity peak 0.5mL	-0.89	0.37
Intensity peak discretized volume sought 1mL	-0.87	0.38
Histogram global intensity peak 1mL	-1.23	0.21
GLCM joint maximum	-0.552	0.58
GLCM joint average	-0.209	0.83
GLCM joint variance	0.74	0.46
GLCM joint entropy $\log^{2}$	-0.43	0.66
GLCM joint entropy $\log^{10}$	-0.43	0.66
GLCM difference average	0.51	0.61
GLCM difference variance	0.36	0.72
GLCM difference entropy	-0.43	0.66
GLCM sum average	-0.209	0.83
GLCM sum variance	-0.971	0.33
GLCM sum entropy	-0.43	0.66

Table 1. Continued

Variable	Test statistics z_R	p-value
GLCM angular second moment	0.47	0.63
GLCM contrast	0.36	0.71
GLCM dissimilarity	0.51	0.61
GLCM inverse difference	-0.36	0.72
GLCM normalised inverse difference	-0.51	0.61
GLCM inverse difference moment	-0.32	0.75
GLCM normalised inverse difference moment	-0.4	0.68
GLCM inverse variance	-0.55	0.58
GLCM correlation	-1.04	0.29
GLCM autocorrelation	-0.171	0.86
GLCM cluster tendency	-0.97	0.33
GLCM cluster shade	-0.47	0.63
GLCM cluster prominence	-0.85	0.39
GLRLM short runs emphasis	0.362	0.71
GLRLM long runs emphasis	-0.43	0.66
GLRLM low grey level run emphasis	-0.43	0.66
GLRLM high grey level run emphasis	-0.28	0.77
GLRLM short run low grey level emphasis	-0.095	0.92
GLRLM short run high grey level emphasis	-0.43	0.66
GLRLM long run low grey level emphasis	-0.476	0.63
GLRLM long run high grey level emphasis	-0.81	0.41
GLRLM grey level non uniformity	-0.704	0.48
GLRLM run length non uniformity	-1.047	0.29
GLRLM run percentage	0.209	0.83
NGTDM coarseness	0.72	0.47
NGTDM contrast	-0.209	0.83
NGTDM busyness	-0.78	0.43
NGTDM complexity	4	0.68
NGTDM strength	0.81	0.41
GLSZM small zone emphasis	1.8	0.07
GLSZM large zone emphasis	-0.85	0.39
GLSZM low gray leve lzone emphasis	-0.43	0.66
GLSZM high gray level zone emphasis	-0.13	0.89
GLSZM small zone low grey level emphasis	-0.24	0.804
GLSZM small zone high grey level emphasis	0.17	0.86
GLSZM large zone low grey level emphasis	-0.62	0.52
GLSZM large zone high grey level emphasis	-1.04	0.29
GLSZM grey level non-uniformity	-0.66	0.51
GLSZM normalized grey level non-uniformity	0.895	0.37
GLSZM zone size non-uniformity	-0.7	0.48
GLSZM normalized zone size non-uniformity	1.808	0.07
GLSZM zone percentage	0.704	0.48

Table 1. Continued		
Variable	**Test statistics z_R**	**p-value**
GLSZM grey level variance	-0.74	0.46
GLSZM zone size variance	-0.704	0.48
GLSZM zone size entropy	-2.3	0.02
GLCM: Grey Level Co-occurrence Matrix, GLRLM: Gray Level Run Length Matrix, NGTDM: Neighbourhood gray-tone difference matrix, GLSZM: Grey Level Size Zone Matrix		

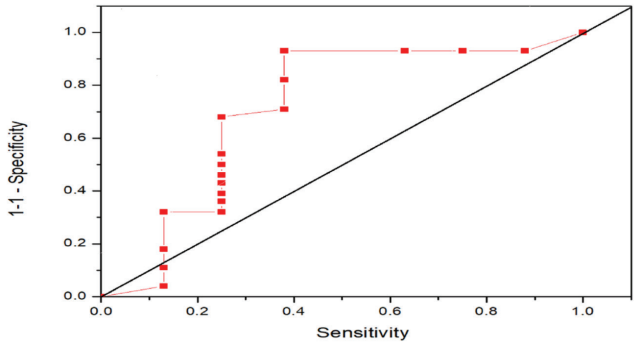

Figure 3. ROC curve for GLSZM-Small Zone Emphasis and GLSZM-Normalized Zone Size Non-Uniformity

ROC: Receiver operating characteristic, GLSZM: Grey Level Size Zone Matrix

features from their study aligned with our findings. Conversely, İnce et al. (12) conducted a study with a larger cohort comprising 82 HCC patients (65 responders and 17 non-responders). They analyzed 1128 radiomic features extracted from pretreatment contrast-enhanced T1-weighted MRI scans obtained within three months before Y-90 treatment. Employing machine learning models, they identified eight radiomic features (including four first-order features, such as kurtosis, three GLCM features, and one shape feature) as optimal predictors for treatment response. Interestingly, one significant feature from their study (Kurtosis) corroborates our findings. Table 4 presents a comparison between previous studies and our current investigation.

Other studies have explored the Y-90 treatment response for HCC or other liver malignancies using diverse imaging modalities(15-17). Reimer et al. (15) assessed the efficacy of texture analysis based on post-treatment MRI of liver metastases in 37 patients to predict response to Y-90 radioembolization during follow-up for colon cancer. They exclusively utilized first-order histogram features, with Kurtosis being the sole feature aligning with our current study. Blanc-Durand et al. (16) employed whole-liver radiomics to devise a scoring system predicting progression-free survival and overall survival in unresectable HCC patients undergoing Y-90 radioembolization. Utilizing 39 imaging features, they developed a two-predictive scoring system categorizing HCC patients into low- and high-risk subgroups in a retrospective cohort of 47 patients. Key radiomics features in their predictive model included variance and NGTDM strength, mirroring aspects of our study. In a separate study, Wei et al. (17) utilized a cohort

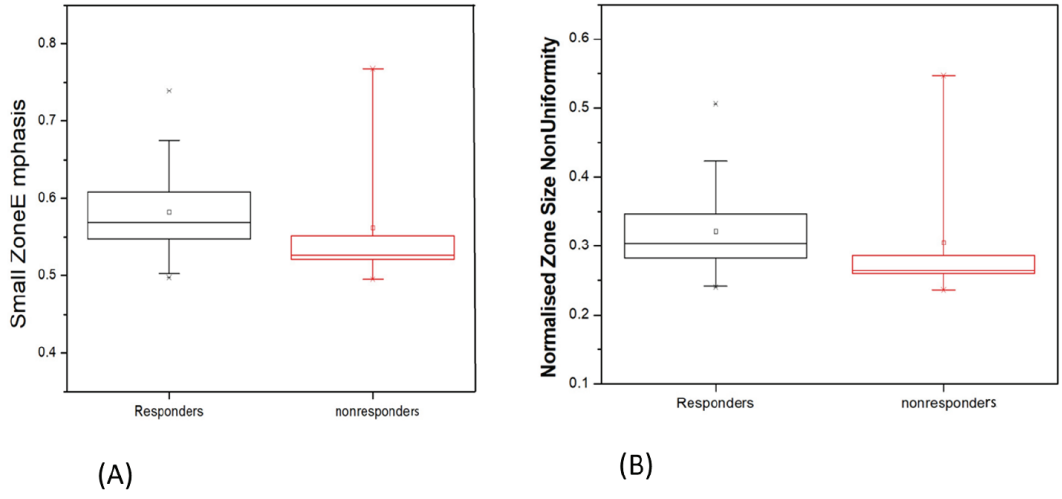

Figure 4. Box plot of (A) GLSZM-Small Zone Emphasis and (B) GLSZM-Normalized Zone Size Non-Uniformity

GLSZM: Grey Level Size Zone Matrix

Table 2. Area under curve (AUC) as calculated from ROC. The below cell shows the features with a good agreement level to differentiate between responders and non-responders. Where green cells show the features with acceptable discrimination values

			Asymptotic Sig.	
Variable	**Area**	**Std. Error**	**Upper bound**	**Lower bound**
Intensity histogram mean	0.5	0.11	1	0.32
Intensity histogram variance	0.42	0.1	0.493	0.25
Intensity histogram skewness	0.53	0.1	0.819	0.37
Intensity histogram kurtosis	0.64	0.11	0.223	0.46
Intensity histogram median	0.52	0.11	0.894	0.34
Intensity histogram 10^{th} percentile	0.58	0.11	0.493	0.4
Intensity histogram 25^{th} percentile	0.56	0.1	0.594	0.4
Intensity histogram 50^{th} percentile	0.52	0.11	0.894	0.34
Intensity histogram75^{th} percentile	0.48	0.11	0.849	0.3
Intensity histogram 90^{th} percentile	0.45	0.11	0.662	0.27
Intensity histogram standard deviation	0.42	0.1	0.493	0.25
Intensity histogram modei	0.47	0.11	0.775	0.29
Intensity histogram mean absolute deviation	0.39	0.11	0.361	0.22
Intensity histogram robust mean absolute deviation	0.42	0.11	0.493	0.24
Intensity histogram median absolute deviation	0.42	0.1	0.518	0.25
Intensity histogram coefficient of variation	0.37	0.11	0.27	0.2
Intensity histogram quartile coefficient of dispersion	0.37	0.11	0.254	0.19
Intensity histogram entropy $\log^{10}$	0.42	0.1	0.47	0.24
Intensity histogram entropy $\log^{2}$	0.42	0.1	0.47	0.24
Intensity histogram area under curve	0.43	0.12	0.568	0.24
Intensity histogram uniformity	0.59	0.11	0.424	0.42
Intensity histogram root mean square	0.66	0.13	0.183	0.44
Intensity histogram maximum histogram gradient	0.43	0.12	0.568	0.23
Intensity histogram maximum histogram gradient grey level	0.5	0.1	0.985	0.33
Intensity histogram minimum histogram gradient	0.57	0.12	0.543	0.37
Intensity histogram minimum histogram gradient grey level	0.5	0.11	1	0.32
Histogram intensity peak discretized volume sought	0.54	0.11	0.746	0.36
Histogram global intensity peak 0.5mL	0.4	0.12	0.381	0.2
Intensity peak discretized volume sought 1mL	0.4	0.1	0.392	0.23
Histogram global intensity peak 1mL	0.36	0.13	0.223	0.15
GLCM joint maximum	0.44	0.1	0.594	0.28
GLCM joint average	0.48	0.11	0.849	0.3
GLCM joint variance	0.42	0.1	0.47	0.25
GLCM joint entropy $\log^{2}$	0.45	0.11	0.676	0.27
GLCM joint entropy $\log^{10}$	0.45	0.11	0.676	0.27
GLCM difference average	0.56	0.12	0.594	0.37
GLCM difference variance	0.54	0.12	0.704	0.35
GLCM difference entropy	0.45	0.11	0.676	0.27
GLCM sum average	0.48	0.11	0.849	0.3

Table 2. Continued

			Asymptotic Sig.	
Variable	**Area**	**Std. Error**	**Upper bound**	**Lower bound**
GLCM sum variance	0.39	0.1	0.341	0.22
GLCM sum entropy	0.45	0.11	0.676	0.27
GLCM angular second moment	0.56	0.1	0.621	0.39
GLCM contrast	0.54	0.11	0.704	0.36
GLCM dissimilarity	0.56	0.12	0.594	0.37
GLCM inverse difference	0.46	0.11	0.732	0.27
GLCM normalised inverse difference	0.44	0.12	0.621	0.25
GLCM inverse difference moment	0.46	0.11	0.761	0.28
GLCM normalised inverse difference moment	0.46	0.11	0.704	0.27
GLCM inverse variance	0.44	0.1	0.594	0.28
GLCM correlation	0.38	0.13	0.304	0.17
GLCM autocorrelation	0.48	0.11	0.879	0.3
GLCM cluster tendency	0.39	0.1	0.341	0.22
GLCM cluster shade	0.45	0.12	0.648	0.25
GLCM cluster prominence	0.4	0.1	0.403	0.24
GLRLM short runs emphasis	0.54	0.12	0.704	0.35
GLRLM long runs emphasis	0.45	0.11	0.676	0.27
GLRLM low grey level run emphasis	0.45	0.11	0.676	0.27
GLRLM high grey level run emphasis	0.49	0.11	0.909	0.31
GLRLM short run low grey level emphasis	0.47	0.11	0.79	0.28
GLRLM short run high grey level emphasis	0.49	0.11	0.939	0.31
GLRLM long run low grey level emphasis	0.45	0.11	0.648	0.27
GLRLM long run high grey level emphasis	0.41	0.1	0.424	0.23
GLRLM grey level non uniformity	0.42	0.13	0.493	0.21
GLRLM run length non uniformity	0.38	0.13	0.304	0.16
GLRLM run percentage	0.53	0.11	0.819	0.34
NGTDM coarseness	0.59	0.13	0.458	0.38
NGTDM contrast	0.48	0.11	0.849	0.3
NGTDM busyness	0.41	0.13	0.447	0.2
NGTDM complexity	0.55	0.11	0.676	0.36
NGTDM strength	0.6	0.14	0.403	0.37
GLSZM small zone emphasis	0.71	0.13	0.068	0.51
GLSZM large zone emphasis	0.4	0.12	0.403	0.2
GLSZM low gray leve lzone emphasis	0.45	0.11	0.676	0.27
GLSZM high gray level zone emphasis	0.49	0.11	0.909	0.3
GLSZM small zone low grey level emphasis	0.47	0.11	0.819	0.29
GLSZM small zone high grey level emphasis	0.52	0.12	0.849	0.33
GLSZM large zone low grey level emphasis	0.43	0.11	0.543	0.24
GLSZM large zone high grey level emphasis	0.38	0.12	0.304	0.19
GLSZM grey level non-uniformity	0.42	0.13	0.518	0.2
GLSZM normalised grey level non-uniformity	0.61	0.11	0.361	0.43

Table 2. Continued				
			Asymptotic Sig.	
Variable	**Area**	**Std. Error**	**Upper bound**	**Lower bound**
GLSZM zone size non-uniformity	0.42	0.13	0.493	0.2
GLSZM normalised zone size non-uniformity	0.71	0.13	0.068	0.51
GLSZM zone percentage	0.58	0.12	0.47	0.39
GLSZM grey level variance	0.42	0.11	0.47	0.24
GLSZM zone size variance	0.42	0.12	0.493	0.23
GLSZM zone size entropy	0.23	0.13	0.022	0.02

ROC: Receiver operating characteristic, GLCM: Grey Level Co-occurrence Matrix, GLRLM: Gray Level Run Length Matrix, NGTDM: Neighbourhood gray-tone difference matrix, GLSZM: Grey Level Size Zone Matrix

Table 3. Cut-off values for the two highest significant features obtained using the maximum Youden index				
Feature	**Cut-off value**	**Sensitivity**	**Specificity**	**Yudin index**
GLSZM-Small Zone Emphasis	0.53	0.93	0.62	0.51
GLSZM-Normalised Zone Size Non-Uniformity	0.27	0.93	0.62	0.55

GLSZM: Grey Level Size Zone Matrix

Table 4. Summarized comparison between the current study and previous studies			
Factor/study	**Aujay et al. (2022) (11)**	**İnce et al. (2023) (12)**	**Current study**
Treatment type	Y-90 (glass+resin)	Y-90 (glass+resin)	Y-90 (glass+resin)
Patients population	22(5 glass, 17 resin)	82 (54 glass, 28 resin)	36 (19 glass, 17 resin)
Response	Responders= 14, Non-responders= 8	Responders= 65, Non-responders= 17	Responders= 28, Non-responders= 8
MRI phase	Arterial phase and portal venous phase MRI one month before and one month after treatment	contrast-enhanced T1-weighted MRI within 3 months before treatment	T2- MRI at the same day of receiving treatment
Post processing			
Number of Feature extracted	107	1.128	86 (the software extract 165 feature but some have errors and some not applicable on MRI so 86 features only included on the statistical work)
Number of significance features	4 (from the post arterial images pre and portal phase was non significance)	8 features	2 features
The most significant feature	GLRLM Long run emphasis With AUC= 1	Combined the 8 radiomics feature with 4 clinical feature to make 4 machine learning model models accuracy for the model between 80-87%	GLSZM-small zone emphasis, and GLSZM-normalized zone size non-uniformity with AUC= 0.71

MRI: Magnetic resonance imaging, GLSZM: Grey Level Size Zone Matrix, AUC: Area under curve,

of 30 patients with primary and secondary liver tumors treated with Y-90 and employed radiomics derived from Y-90 PET to predict treatment response. They identified 15 significant features, including NGTDM strength, consistent with our findings.

Discrepancies in features may stem from variations in sample size and the statistical analysis methodology. Additionally, radiomics holds promise in enhancing medical diagnosis, yet studies have uncovered variability in radiomics values due to several factors. These factors include the voxel size

(18,19), the algorithms used for reconstruction (20,21), the methods used for tumor segmentation (22,23), and the discretization of grey-level values (24,25). This variability in radiomics values can pose a challenge to the accuracy and reliability of radiomics-based diagnosis.

Study Limitations

The current study has certain limitations worth noting, such as a relatively small sample size, a restricted number of radiomic features analyzed, and absence of a comparison between our findings and other clinical information, such as histopathology results. Furthermore, we did not correlate the radiomics results with the clinical progression of the disease or liver function parameters. However, it's essential to emphasize that the primary objective of this study was to explore the predictive capacity of radiomics in determining Y-90 treatment response, with plans to expand upon these findings in our future research endeavors.

Conclusion

In conclusion, this study shows that radiomics extracted from MRI-T2 images could be used as a non-invasive tool for predicting the response of HCC to Y-90 treatment. Two radiomic features, "GLSZM-Small Zone Emphasis" and "GLSZM-Normalized Zone Size Non-Uniformity", were found to have the highest discrimination ability for differentiating responders from non-responders.

Ethics

Ethics Committee Approval: This study protocol was reviewed and approved by the Ethics Committee of Taipei Veterans General Hospital (IRB no: 2020-04-013BC, date: 13.04.2020). Informed consent was obtained from all subjects during inclusion in the study.

Informed Consent: Informed consent was obtained from all individual participants included in the study.

Authorship Contributions

Surgical and Medical Practices: M.M., K.H.L., R.C.L., Concept: M.M., Design: M.M., K.H.L., Data Collection or Processing: M.M., K.H.L., R.C.L., C.L., Analysis or Interpretation: M.M., K.H.L., R.C.L., C.L., Literature Search: M.M., Writing: M.M., K.H.L.

Conflict of Interest: No conflict of interest was declared by the authors.

Financial Disclosure: The authors declared that this study has received no financial support.

References

1. El-Serag HB. Hepatocellular carcinoma. N Engl J Med. 2011;365:1118-1127.
2. Salem R, Lewandowski RJ, Kulik L, Wang E, Riaz A, Ryu RK, Sato KT, Gupta R, Nikolaidis P, Miller FH, Yaghmai V, Ibrahim SM, Senthilnathan S, Baker T, Gates VL, Atassi B, Newman S, Memon K, Chen R, Vogelzang RL, Nemcek AA, Resnick SA, Chrisman HB, Carr J, Omary RA, Abecassis M, Benson AB 3rd, Mulcahy MF. Radioembolization results in longer time-to-progression and reduced toxicity compared with chemoembolization in patients with hepatocellular carcinoma. Gastroenterology. 2011;140:497-507.
3. Kang TW, Kim JM, Rhim H, Lee MW, Kim YS, Lim HK, Choi D, Song KD, Kwon CH, Joh JW, Paik SW, Paik YH, Ahn JH. Small Hepatocellular Carcinoma: Radiofrequency Ablation versus Nonanatomic Resection--Propensity Score Analyses of Long-term Outcomes. Radiology. 2015;275:908-919.
4. Lencioni R, Llovet JM. Modified RECIST (mRECIST) assessment for hepatocellular carcinoma. Semin Liver Dis. 2010;30:52-60.
5. Aerts HJ, Velazquez ER, Leijenaar RT, Parmar C, Grossmann P, Carvalho S, Bussink J, Monshouwer R, Haibe-Kains B, Rietveld D, Hoebers F, Rietbergen MM, Leemans CR, Dekker A, Quackenbush J, Gillies RJ, Lambin P. Decoding tumour phenotype by noninvasive imaging using a quantitative radiomics approach. Nat Commun. 2014;5:4006.
6. Kong C, Zhao Z, Chen W, Lv X, Shu G, Ye M, Song J, Ying X, Weng Q, Weng W, Fang S, Chen M, Tu J, Ji J. Prediction of tumor response via a pretreatment MRI radiomics-based nomogram in HCC treated with TACE. Eur Radiol. 2021;31:7500-7511.
7. Zhao Y, Wang N, Wu J, Zhang Q, Lin T, Yao Y, Chen Z, Wang M, Sheng L, Liu J, Song Q, Wang F, An X, Guo Y, Li X, Wu T, Liu AL. Radiomics Analysis Based on Contrast-Enhanced MRI for Prediction of Therapeutic Response to Transarterial Chemoembolization in Hepatocellular Carcinoma. Front Oncol. 2021;11:582788.
8. Kuang Y, Li R, Jia P, Ye W, Zhou R, Zhu R, Wang J, Lin S, Pang P, Ji W. MRI-Based Radiomics: Nomograms predicting the short-term response after transcatheter arterial chemoembolization (TACE) in hepatocellular carcinoma patients with diameter less than 5 cm. Abdom Radiol (NY). 2021;46:3772-3789.
9. Tian Y, Komolafe TE, Chen T, Zhou B, Yang X. Prediction of TACE Treatment Response in a Preoperative MRI via Analysis of Integrating Deep Learning and Radiomics Features. J Med Biol Eng. 2022;42:169-178.
10. Liu QP, Yang KL, Xu X, Liu XS, Qu JR, Zhang YD. Radiomics analysis of pretreatment MRI in predicting tumor response and outcome in hepatocellular carcinoma with transarterial chemoembolization: a two-center collaborative study. Abdom Radiol (NY). 2022;47:651-663.
11. Aujay G, Etchegaray C, Blanc JF, Lapuyade B, Papadopoulos P, Pey MA, Bordenave L, Trillaud H, Saut O, Pinaquy JB. Comparison of MRI-based response criteria and radiomics for the prediction of early response to transarterial radioembolization in patients with hepatocellular carcinoma. Diagn Interv Imaging. 2022;103:360-366.
12. İnce O, Önder H, Gençtürk M, Cebeci H, Golzarian J, Young S. Prediction of Response of Hepatocellular Carcinoma to Radioembolization: Machine Learning Using Preprocedural Clinical Factors and MR Imaging Radiomics. J Vasc Interv Radiol. 2023;34:235-243.
13. Nioche C, Orlhac F, Boughdad S, Reuzé S, Goya-Outi J, Robert C, Pellot-Barakat C, Soussan M, Frouin F, Buvat I. LIFEx: A Freeware for Radiomic Feature Calculation in Multimodality Imaging to Accelerate Advances in the Characterization of Tumor Heterogeneity. Cancer Res. 2018;78:4786-4789.
14. Lencioni R, Llovet JM. Modified RECIST (mRECIST) assessment for hepatocellular carcinoma. Semin Liver Dis. 2010;30:52-60.
15. Reimer RP, Reimer P, Mahnken AH. Assessment of Therapy Response to Transarterial Radioembolization for Liver Metastases by Means of

Post-treatment MRI-Based Texture Analysis. Cardiovasc Intervent Radiol. 2018;41:1545-1556.

16. Blanc-Durand P, Van Der Gucht A, Jreige M, Nicod-Lalonde M, Silva-Monteiro M, Prior JO, Denys A, Depeursinge A, Schaefer N. Signature of survival: a ^{18}F-FDG PET based whole-liver radiomic analysis predicts survival after ^{90}Y-TARE for hepatocellular carcinoma. Oncotarget. 2018;9:4549-4558.
17. Wei L, Cui C, Xu J, Kaza R, El Naqa I, Dewaraja YK. Tumor response prediction in ^{90}Y radioembolization with PET-based radiomics features and absorbed dose metrics. EJNMMI Phys. 2020;7:74.
18. Shafiq-Ul-Hassan M, Zhang GG, Latifi K, Ullah G, Hunt DC, Balagurunathan Y, Abdalah MA, Schabath MB, Goldgof DG, Mackin D, Court LE, Gillies RJ, Moros EG. Intrinsic dependencies of CT radiomic features on voxel size and number of gray levels. Med Phys. 2017;44:1050-1062.
19. Shafiq-Ul-Hassan M, Latifi K, Zhang G, Ullah G, Gillies R, Moros E. Voxel size and gray level normalization of CT radiomic features in lung cancer. Sci Rep. 2018;8:10545.
20. Altazi BA, Zhang GG, Fernandez DC, Montejo ME, Hunt D, Werner J, Biagioli MC, Moros EG. Reproducibility of F18-FDG PET radiomic features for different cervical tumor segmentation methods, gray-level discretization, and reconstruction algorithms. J Appl Clin Med Phys. 2017;18:32-48.
21. van Velden FH, Kramer GM, Frings V, Nissen IA, Mulder ER, de Langen AJ, Hoekstra OS, Smit EF, Boellaard R. Repeatability of Radiomic Features in Non-Small-Cell Lung Cancer [(18)F]FDG-PET/CT Studies: Impact of Reconstruction and Delineation. Mol Imaging Biol. 2016;18:788-795.
22. Qiu Q, Duan J, Duan Z, Meng X, Ma C, Zhu J, Lu J, Liu T, Yin Y. Reproducibility and non-redundancy of radiomic features extracted from arterial phase CT scans in hepatocellular carcinoma patients: impact of tumor segmentation variability. Quant Imaging Med Surg. 2019;9:453-464.
23. Haniff NSM, Abdul Karim MK, Osman NH, Saripan MI, Che Isa IN, Ibahim MJ. Stability and Reproducibility of Radiomic Features Based Various Segmentation Technique on MR Images of Hepatocellular Carcinoma (HCC). Diagnostics (Basel). 2021;11:1573.
24. Duron L, Balvay D, Vande Perre S, Bouchouicha A, Savatovsky J, Sadik JC, Thomassin-Naggara I, Fournier L, Lecler A. Gray-level discretization impacts reproducible MRI radiomics texture features. PLoS One. 2019;14:e0213459.
25. Mahmoud M, Shihab M, Saad S, Elhussiny F, Houseni M. Imaging differentiation of malignant hepatic tumors: Radiomics and metabolic features of ^{18}F-FDG PET/CT. Russ Electron J Radiol. 2021;11:165-170.